

# Knockdown of TFAP2E results in rapid G<sub>2</sub>/M transition in oral squamous cell carcinoma cells

RYO SAKAI<sup>1,2</sup>, KYOKO FUJIWARA<sup>3,4</sup>, ERI NAGASAKI-MAEOKA<sup>5</sup>, YOSHINORI INAGAKI<sup>6</sup>,  
BIN YAMAOKA<sup>7</sup>, ERI MUTO-FUJITA<sup>7</sup>, YUSUKE KAMIDAKI<sup>7</sup>, TSUGUMICHI KOSHINAGA<sup>7</sup>,  
SHUICHIRO UEHARA<sup>7</sup>, TADATERU TAKAYAMA<sup>6</sup> and SHUICHI SATO<sup>2,8</sup>

<sup>1</sup>Department of Periodontology, Nihon University School of Dentistry; <sup>2</sup>Division of Applied Oral Science, Nihon University Graduate School of Dentistry; <sup>3</sup>Department of Anatomy; <sup>4</sup>Division of Functional Morphology, Dental Research Center, Nihon University School of Dentistry, Tokyo 101-8310; <sup>5</sup>Department of Pediatric Surgery, Jichi Medical University, Saitama Medical Center, Saitama 330-8503; <sup>6</sup>Division of General Medicine, Department of Medicine; <sup>7</sup>Department of Pediatric Surgery, Nihon University School of Medicine, Tokyo 173-0032; <sup>8</sup>Division of Advanced Dental Treatment, Dental Research Center, Nihon University School of Dentistry, Tokyo 101-8310, Japan

Received October 20, 2023; Accepted January 11, 2024

DOI: 10.3892/ol.2024.14260

**Abstract.** TFAP2E is a member of the activator protein-2 transcription factor family and acts as a tumor suppressor in several types of cancer. Downregulation of TFAP2E expression is significantly associated with a shorter overall survival period in patients with oral squamous cell carcinoma (OSCC). To evaluate the molecular mechanisms by which TFAP2E suppresses the development or progression of OSCC, the present study investigated the effects of TFAP2E downregulation on OSCC-derived Ca9-22 and HSC-4 cells. The present study demonstrated that small interfering RNA mediated-knockdown of TFAP2E accelerated the proliferation of these OSCC cell lines compared with that in the control group, as determined by the standard water-soluble tetrazolium salt-8 assay. To analyze the cell cycle progression rate, the cell cycle distribution patterns of TFAP2E-knockdown and control cells cultured in the presence of nocodazole, which prevents the completion of mitosis, were analyzed by fluorescence-activated cell sorting at different time points. When analyzing cellular DNA contents, no major differences in cell cycle profiles were observed; however, the rate of increase in cells positive for histone H3 Serine 28 phosphorylation, a standard molecular marker of early M phase, was significantly higher in TFAP2E-knockdown cells than in the control cells. Collectively, these results suggested that TFAP2E may

attenuate the proliferation of OSCC cells by regulating G<sub>2</sub>/M transition.

## Introduction

Head and neck squamous cell carcinoma (HNSCC) is the eighth most common malignancy worldwide, with ~878,000 new cases and ~444,000 deaths recorded in 2020 (1). The most common type of HNSCC is oral squamous cell carcinoma (OSCC), which is characterized by malignancies that develop in the oral cavity and on the lips. OSCC had a global annual incidence of 378,000 and 178,000 annual deaths in 2020 (1). These numbers are markedly higher than the 300,000 new cases and 145,000 deaths reported in 2015 (2). Despite the development of novel therapeutic strategies, the 5-year survival rate of patients with OSCC is ~70% (3). OSCC mainly occurs on the tongue, lips and oral floor; appearing as ulcers, lumps or lesions with aberrant color. Tobacco and alcohol consumption are primary risk factors for OSCC (4), and other factors, such as betel quid chewing, diet, irradiation and infection with high-risk types of human papilloma virus (HPV), have been implicated. Comprehensive analyses have identified genomic alterations in HNSCC, including OSCC, some of which are etiologically specific (5). For example, HNSCC that develops in smokers commonly shows specific mutations in TP53 and inactivation of CDKN2A, whereas mutations in these genes are rarely observed in HPV-positive HNSCC (5). However, the precise molecular mechanisms underlying the development and progression of OSCC remain unclear.

In our previous study, we screened for aberrantly methylated genomic regions in a mouse model of skin SCC induced by a two-stage chemical carcinogenesis protocol. The results showed that the methylation level of CpG islands (CpGi) in intron 3 of TFAP2E was significantly elevated, and the expression levels of TFAP2E were markedly reduced in mouse skin SCC compared with those in normal skin (6). TFAP2E encodes

*Correspondence to:* Dr Kyoko Fujiwara, Department of Anatomy, Nihon University School of Dentistry, 1-8-13 Kanda-Surugadai, Chiyoda-ku, Tokyo 101-8310, Japan  
E-mail: fujiwara.kyoko@nihon-u.ac.jp

**Key words:** oral squamous cell carcinoma, TFAP2E, cell cycle, G<sub>2</sub>/M transition

nuclear transcription factor activator protein-2 (AP-2) $\epsilon$ . The AP-2 family consists of five members, TFAP2A, TFAP2B, TFAP2C, TFAP2D and TFAP2E, all of which share highly conserved structures, such as an  $\alpha$ -helical DNA-binding domain and a helix-span-helix motif. They have been shown to serve pivotal roles in the regulation of early development, as well as in carcinogenesis (7,8). During embryogenesis in mice, TFAP2E is mainly expressed in neural tissues (9), and is involved in the development of the olfactory bulb (10) and retina (11). TFAP2E is also expressed during chondrocyte differentiation in both mice (12) and humans where it regulates the expression of integrin  $\alpha$ 10 (13).

Accumulating evidence has suggested that TFAP2E acts as a tumor suppressor in several types of cancer. In humans, the TFAP2E gene is located on chromosome 1p34, a genetic region that is deleted in numerous types of cancer (14). Similar to the observations in mice (6), hypermethylation of the CpG in intron 3 of human TFAP2E has been observed to be associated with decreased TFAP2E transcription level, and nonresponse to 5-fluorouracil (5-FU) in colorectal cancer (CRC) and gastric cancer (GC) (15,16). In addition, hypermethylation of TFAP2E is more frequently detected in urinary genomic DNA obtained from patients with prostate cancer than from young healthy male subjects (17). Our previous study reported that lower levels of TFAP2E expression are significantly associated with shorter survival in patients with neuroblastoma (NB) (18). Collectively, these findings strongly suggested that TFAP2E is a potential tumor suppressor.

The present study examined the possible role of TFAP2E in the development or progression of OSCC. For this purpose, the effects of TFAP2E knockdown on the viability and cell cycle progression of OSCC cells were analyzed.

## Materials and methods

**Cell lines and culture conditions.** The human gingival cancer cell line Ca9-22 was obtained from the Japanese Collection of Research Bioresources Cell Bank and the human tongue cancer-derived cell line HSC-4 was obtained from the RIKEN BioResource Center. As it has been reported that some stocks of Ca9-22 are contaminated with MSK-922 (19), short tandem repeat analysis was performed for the Ca9-22 cell line by BEX Co., Ltd., and it was confirmed to be authentic. Ca9-22 cells were cultured in minimal essential medium (Nacalai Tesque, Inc.) supplemented with 600 mg/l glutamine and 10% heat-inactivated fetal bovine serum (FBS; Nichirei Biosciences, Inc.). HSC-4 cells were maintained in RPMI-1640 medium (Nacalai Tesque, Inc.) supplemented with 10% heat-inactivated FBS. Both media contained 100 IU/ml penicillin (Thermo Fisher Scientific, Inc.) and 100 mg/ml streptomycin (Thermo Fisher Scientific, Inc.). Cells were maintained at 37°C in an atmosphere containing 95% air and 5% CO<sub>2</sub>.

**Kaplan-Meier survival analysis.** To assess the effects of expression levels of TFAP2E on the survival rate of patients with OSCC, Kaplan-Meier survival analysis, followed by log-rank test for statistical analysis, was performed using the online cBioPortal tool (<http://www.cbioportal.org>). Sample data from 322 patients in The Cancer Genome Atlas (TCGA) HNSCC Firehose Legacy data set, including gene expression

levels in OSCC tissues and survival period, were obtained from cBioPortal.

**Small interfering RNA (siRNA)-mediated knockdown of TFAP2E.** Ca9-22 and HSC-4 cells were seeded and cultured for 24 h before transfecting with 10 nM siRNA using Lipofectamine<sup>®</sup> 3000 (Invitrogen; Thermo Fisher Scientific, Inc.), according to the manufacturer's instructions at room temperature. Anti-TFAP2E siRNA (cat. no. s50548; Thermo Fisher Scientific, Inc.), a control siRNA (si-N/C; cat. no. 4390843; Thermo Fisher Scientific, Inc.) and anti-TP53 siRNA (cat. no. sc-29435; Santa Cruz Biotechnology, Inc.) were used in the present study.

**Analysis of cell proliferation.** To analyze the cell proliferation rate, cells were seeded into 96-well culture plates at a density of 5x10<sup>3</sup> cells/well and transfected with siRNAs after 24 h. After 1, 2, 3, 4 and 5 days, the proliferation of transfected cells was measured using the standard water-soluble tetrazolium salt (WST)-8 assay with Cell Count Reagent CF (Nacalai Tesque, Inc.). Briefly, culture medium was replaced with fresh medium containing 10  $\mu$ l of WST8 solution, and the cells were cultured for 1 h, followed by measurement of the absorbance at 450 nm using a plate reader (Spectra Max ABS plus; Molecular Devices, LLC).

Cell viability was also analyzed by cell staining. Briefly, cells were seeded into 6-well culture plates at a density of 5x10<sup>3</sup> cells/well. A total of 24 h after seeding, cells were transfected with siRNAs and were cultured for 10 days. In the middle of culture, i.e. 5 days after siRNAs transfection, the medium was replaced and siRNA transfection was performed again. Cells were fixed and stained using a Diff-Quick Stain Kit (Sysmex Corporation) at room temperature. Briefly, cells were fixed with 99% methanol for 10 min and stained with Diff-Quick solution II for 5 min, followed by washing with distilled water.

For the analysis of drug sensitivity, cells were seeded into 96-well culture plates at a density of 5x10<sup>3</sup> cells/well and transfected with siRNAs after 24 h. In addition, 1, 5 and 10  $\mu$ M cisplatin (CDDP; MilliporeSigma) or 25, 50 and 100  $\mu$ M of H<sub>2</sub>O<sub>2</sub> (Nacalai Tesque, Inc.) were added 24 h after the transfection, followed by culture for additional 24 h and analysis of cell viability using WST-8 assay.

**Analysis of cell cycle distribution.** The cells were plated at a density of 2x10<sup>4</sup> cells/ml in culture dishes 60 mm in diameter (5 ml/dish) and were transfected with siRNAs 24 h later. A total of 3 days after transfection, both floating and attached cells were collected by centrifugation, washed in PBS and fixed in 70% ethanol at -20°C overnight for fluorescence-activated cell sorting (FACS) analysis. The cells were washed in PBS before incubating in PBS containing 0.1% FBS, 25  $\mu$ g/ml propidium iodide and 200  $\mu$ g/ml RNase A for 15 min at room temperature.

Cell cycle progression was monitored in the presence of nocodazole, which prevents cells from completing mitosis (20). The cells were plated and transfected with siRNAs as aforementioned. After 2 days of culture, the medium was replaced with fresh medium containing 100 ng/ml nocodazole (FUJIFILM Wako Pure Chemical Corporation). The cells were harvested every 3 h and fixed in 70% ethanol at -20°C overnight. The

cells were washed in PBS containing 0.5% FBS, followed by incubation in PBS containing 0.5% FBS, 2.5  $\mu\text{g/ml}$  propidium iodide, 200  $\mu\text{g/ml}$  RNase A and anti-phosphorylated histone H3 serine 28 (p-H3Ser28) conjugated with Alexa 647 (cat. no. 641006; BioLegend, Inc.) for 1 h at room temperature.

All of the aforementioned cells were subjected to FACS analysis using a Gallios Flow Cytometer (Beckman Coulter, Inc.) and data analysis was performed using Kaluza Analysis Software Ver. 2.1 (Beckman Coulter, Inc.). The percentage distribution of cells in distinct cell cycle phases was calculated based on Michael H. Fox algorithm (21).

**Reverse transcription-quantitative RT-qPCR.** Ca9-22 and HSC-4 cells were plated at a density of  $2 \times 10^4$  cells/ml in culture dishes 60 mm in diameter (5 ml/dish) and were transfected with siRNAs 24 h after seeding. Total RNA was extracted from cells 2 or 5 days after siRNA transfection, using RNeasy mini kits (Qiagen GmbH) and cDNA was synthesized by RT using an iScript cDNA synthesis system (Bio-Rad Laboratories, Inc.), according to the manufacturers' instructions. qPCR for TFAP2E and 18S rRNA, which was used as a housekeeping gene (22), was performed using the TaqMan Pre-Developed Assay Reagents Hs00698734\_m1 and Hs99999901\_s1 for TFAP2E and 18S rRNA (Thermo Fisher Scientific, Inc.) respectively, and Premix Ex Taq Perfect Real Time (Takara Bio, Inc.). qPCR conditions were as follows: Initial denaturation at 95°C for 30 sec, followed by 40 cycles at 95°C for 5 sec and 60°C for 30 sec. qPCR for TP53 was performed using SYBR Premix Ex Taq™ (Takara Bio, Inc.) with the following primers: Sense 5'-CCCCTCCTGGCCCCCTGTCATCTTC-3' and antisense 5'-GCAGCGCCTCACAACCTCCGTCAT-3'. qPCR conditions were as follows: Initial denaturation at 95°C for 30 sec, followed by 40 cycles at 95°C for 5 sec, 56°C for 10 sec and 72°C for 30 sec. Measurements were performed in triplicate. Data processing was performed using a standard curve-based method (23). A mixture of cDNA generated from the total RNA of Ca9-22 and HSC-4 cells was used to obtain a standard curve for each gene.

**Western blotting.** Ca9-22 and HSC-4 cells were plated at a density of  $2 \times 10^4$  cells/ml in culture dishes 60 mm in diameter (5 ml/dish) and were transfected with siRNAs 24 h after seeding. Cells were collected 2 days after transfection with siRNAs. For the analysis of cell cycle-related proteins, cells were treated with 100 ng/ml nocodazole 2 days after the transfection and collected 0, 3, 6, 9 and 12 h after nocodazole addition. Cells were lysed in RIPA buffer containing a protease and phosphatase inhibitor cocktail (Nacalai Tesque, Inc.), before passing through a 1-ml syringe with a 27-G needle. Protein concentrations in the lysates were measured using a Bio-Rad DC kit (Bio-Rad Laboratories, Inc.). The lysates containing 10  $\mu\text{g}$  protein were separated by SDS-PAGE on 4-12% gels, followed by electroblotting onto Immobilon-P membranes (MilliporeSigma). Membranes were blocked with Blocking-one (Nacalai Tesque, Inc.) overnight at 4°C and incubated with anti-TFAP2E (cat. no. 29-175; ProSci, Inc.; 1:1,000), anti-Cyclin B1 (D-11; cat. no. sc-7393; Santa Cruz Biotechnology, Inc.; 1:1,000), anti-histone H3 (cat. no. 9715; Cell Signaling Technology, Inc.; 1:1,000), anti-p-H3Ser28 (cat. no. 9713; Cell Signaling Technology, Inc.; 1:1,000),

anti-GAPDH (cat. no. ab9485; Abcam.; 1:1,000) and anti-TP53 (DO-1; cat. no. sc-126; Santa Cruz Biotechnology, Inc.; 1:1,000) antibodies at 4°C. After incubation for 24 h, the membranes were washed in Tris-buffered saline (TBS) containing 0.1% Tween 20 (TBS-T), followed by incubation with the appropriate horseradish peroxidase-conjugated secondary antibodies (cat. nos. NA934V and NA931V; Cytiva; 1:2,000) for 1 h at room temperature. The membranes were washed extensively with TBS-T and the results were visualized using Chemi-Lumi-One Super (Nacalai Tesque, Inc.) and an ImageQuant™ 800 system (Danaher Corp.). Experiments were performed at least three times and representative blots are shown. The band density of histone H3 (total H3) and p-H3Ser28 was semi-quantified using ImageJ (ver. 1.48; National Institutes of Health) (24) to normalize signal intensity of p-H3Ser28 to total H3.

**Statistical analysis.** Statistical analyses to examine the significance of the differences between two groups were performed using Student's unpaired t-test. One-way ANOVA followed by post-hoc Tukey's test was performed to examine the significance of the differences among multiple groups. All statistical analyses were performed using JMP software ver. 11.2 (SAS Institute, Inc.). Data are presented as the mean  $\pm$  SD of at least three independent experiments. In all analyses,  $P < 0.05$  was considered to indicate a statistically significant difference.

## Results

**Low TFAP2E expression is related to poor prognosis of OSCC.** Kaplan-Meier survival analysis of TCGA public microarray data sets was performed for 322 cases, including 128 cases of OSCC in the oral tongue, 27 in the base of the tongue, 62 in the floor of the mouth, 22 in the buccal mucosa, 7 in the hard palate, 3 in the lips and 73 in the oral cavity. The patients were divided to low or high expression groups using the median expression level of TFAP2E as a cutoff. Kaplan-Meier analysis showed that low TFAP2E expression was significantly associated with a shorter overall survival in patients with OSCC (Fig. 1). These results strongly suggested that TFAP2E plays a suppressive role in the malignant progression of OSCC.

**Knockdown of TFAP2E promotes the proliferation of OSCC-derived cells.** To assess the hypothesis that TFAP2E acts as a tumor suppressor in OSCC, the present study examined the effects of TFAP2E knockdown on human OCSS-derived Ca9-22 and HSC-4 cells using anti-TFAP2E siRNA. RT-qPCR and western blotting confirmed that Ca9-22 and HSC-4 cells transfected with anti-TFAP2E siRNA exhibited reduced endogenous TFAP2E expression compared with in the control group (Fig. 2A and B). The standard WST-8 cell survival assay showed that TFAP2E knockdown resulted in a marked increase in cell proliferation (Fig. 2C and D). Consistent with these results, the number of viable TFAP2E-depleted cells was substantially greater than that in the control group (Fig. 2E and F).

The present study also examined whether TFAP2E knockdown affected cell proliferation or cell cycle progression by analyzing the cell cycle distribution of Ca9-22 and HSC-4 cells transfected with anti-TFAP2E siRNA or control siRNA using FACS. There were no significant differences in either



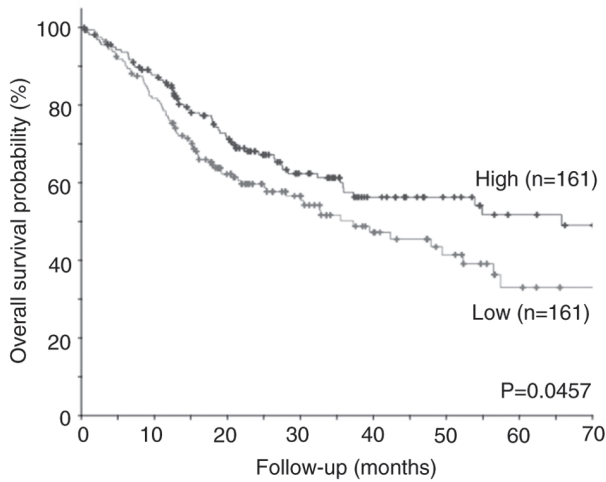


Figure 1. Kaplan-Meier analysis of data from 322 patients with OSCC demonstrated that TFAP2E expression was associated with the survival rate of patients with OSCC. OSCC, oral squamous cell carcinoma.

cell cycle distribution or the proportion of dead cells, as indicated by sub-G<sub>1</sub> DNA content, between TFAP2E-knockdown and control cell groups (Fig. 3). In addition, knockdown of TFAP2E had a negligible effect on the resistance of the cells to CDDP and H<sub>2</sub>O<sub>2</sub> (Fig. S1), indicating that knockdown of TFAP2E may accelerate cell growth via some mechanism other than augmenting stress resistance in the cells.

**Knockdown of TFAP2E results in rapid G<sub>2</sub>/M transition of OSCC cells.** To investigate the mechanisms by which TFAP2E depletion promotes cell proliferation, the present study analyzed the cell cycle progression rate. Because anti-TFAP2E siRNA did not work when cells were treated with a double thymidine block to achieve synchronization to the late G<sub>1</sub> phase (data not shown), cell cycle progression was analyzed using the previously reported method for asynchronous cells (25). In this method, cell cycle progression was monitored in the presence of nocodazole. As nocodazole prevents cells from completing mitosis, cell cycle progression rate could be analyzed by measuring the accumulation rate of G<sub>2</sub>/M cells. FACS analysis showed that the proportion of cells in the G<sub>0</sub>/G<sub>1</sub> phase decreased and that of cells in the G<sub>2</sub>/M phase increased in a time-dependent manner (Figs. 4A, B and S2); however, there were few significant differences between control and TFAP2E-knockdown cells. The G<sub>2</sub> and M phases could not be distinguished based on the DNA content of the cells, since cells in both G<sub>2</sub> and M phase have 4N DNA content (tetraploidy); therefore, the present study also monitored the population of cells positive for p-H3Ser28, which is a reliable marker of the early M phase (26). The proportion of p-H3Ser28-positive cells increased over time, and the rate of increase was significantly higher in TFAP2E-depleted Ca9-22 cells compared with that in the control group (Figs. 4C and S3A); similar results were observed in HSC-4 cells (Figs. 4D and S3B). Consistent with these results, western blotting demonstrated that the accumulation of p-H3Ser28 and cyclin B1, an alternative molecular marker for the G<sub>2</sub>/M phase, occurred earlier in TFAP2E-knockdown cells than in control cells (Fig. 5). Collectively, these results suggested that TFAP2E may serve

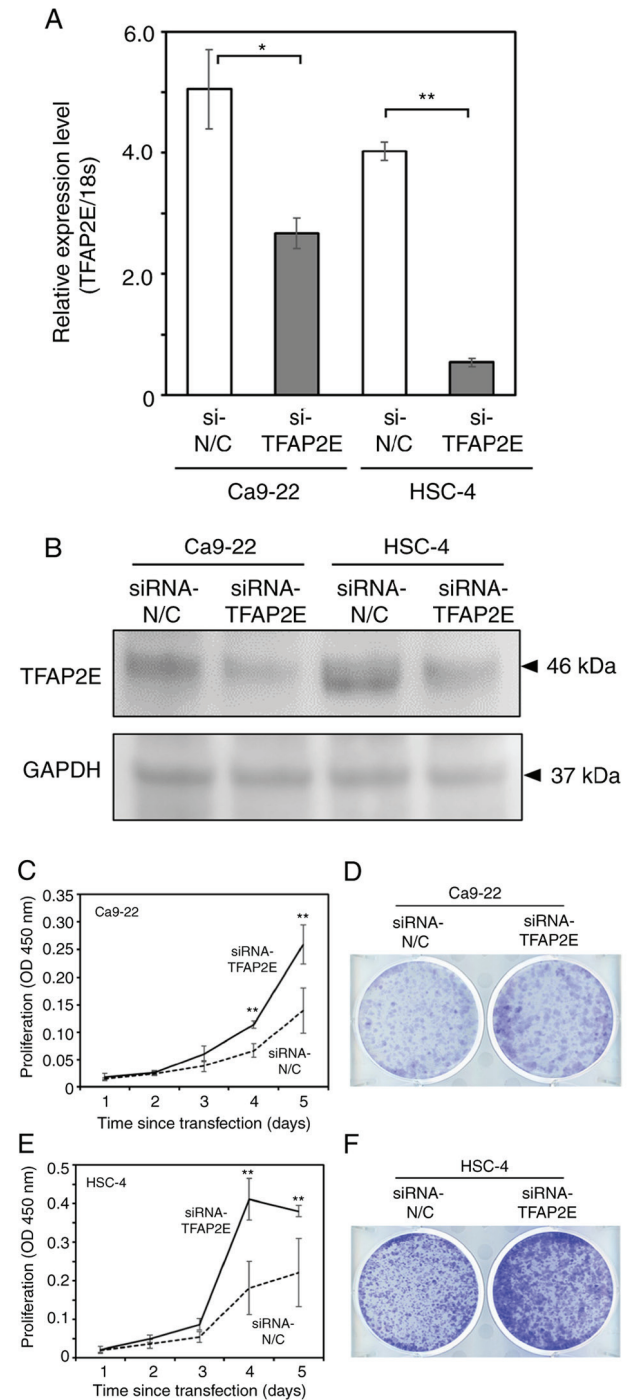


Figure 2. siRNA-mediated knockdown of TFAP2E accelerates OSCC cell proliferation. OSCC-derived Ca9-22 and HSC-4 cells were transfected with si-TFAP2E or si-N/C. A total of 2 days after transfection, total RNA and cell lysates were prepared and analyzed by (A) reverse transcription-quantitative PCR and (B) western blotting, respectively. Data are presented as the mean  $\pm$  SD of triplicate measurements. \* $P$ <0.05, \*\* $P$ <0.01. GAPDH was used as a loading control for western blotting. Proliferation of (C) Ca9-22 and (E) HSC-4 cells was determined by water-soluble tetrazolium salt-8 assay at the indicated time points post-transfection. Data are presented as the mean  $\pm$  SD of quadruplicate measurements. \*\* $P$ <0.01 vs. si-N/C. To visualize viable cells, cells were fixed and stained using a Diff-Quick Stain Kit 10 days after transfection. Representative images of (D) Ca9-22 and (F) HSC-4 are shown. N/C, negative control; siRNA, small interfering RNA.

a role in regulating the G<sub>2</sub>/M transition in OSCC cells. As a tumor suppressor gene TP53 is a key molecule in regulation

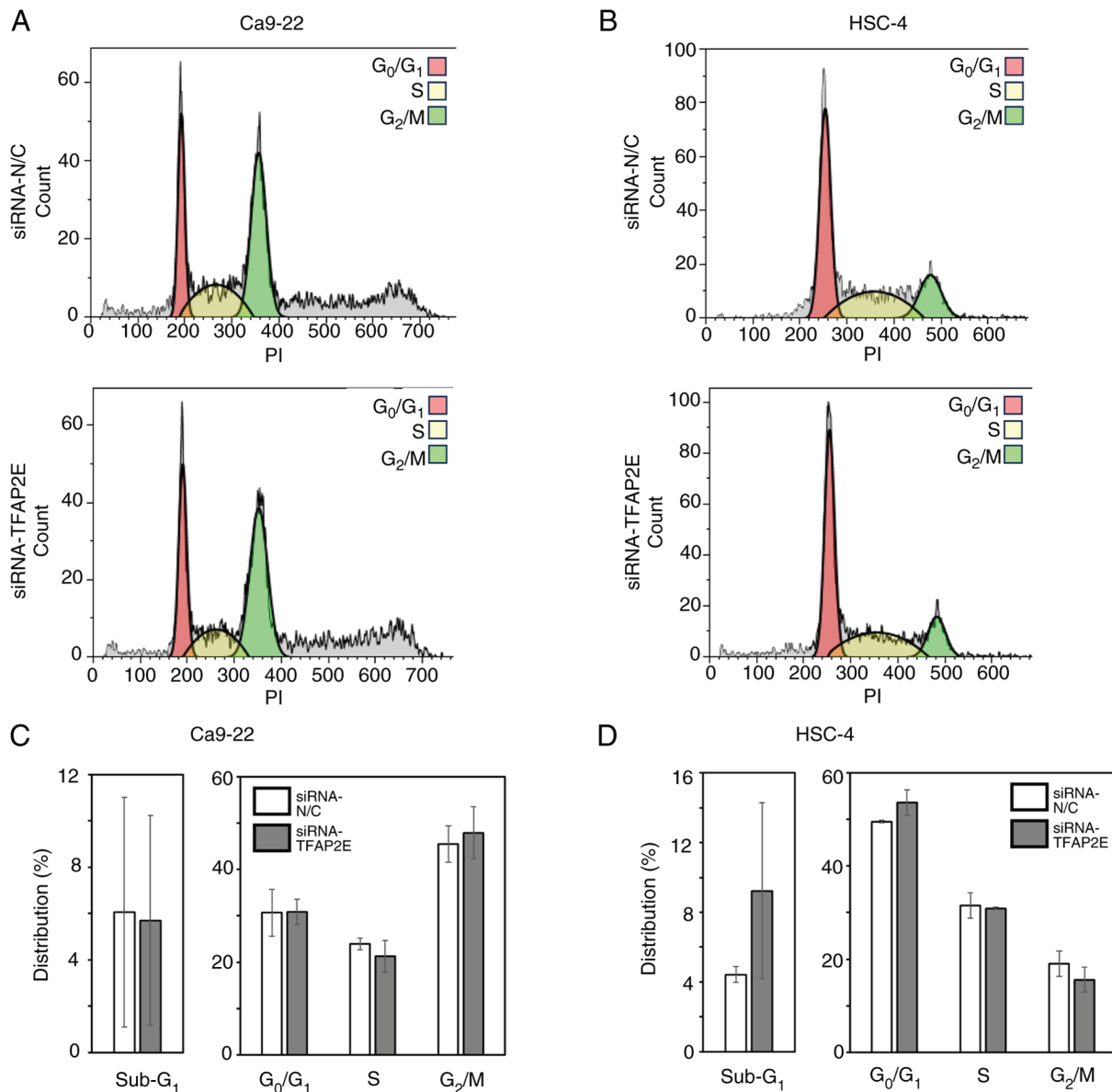


Figure 3. TFAP2E-knockdown has no detectable effect on cell cycle distribution patterns. (A and C) Ca9-22 and (B and D) HSC-4 cells were transfected with siRNA-TFAP2E or siRNA-N/C. A total of 3 days after transfection, floating and adherent cells were harvested and stained with propidium iodide, and their cell cycle distributions were examined using fluorescence-activated cell sorting. The experiments were performed at least three times, and the percentage distribution was calculated based on Michael H. Fox algorithm. (A and B) Representative histograms are shown. (C and D) Data are presented as the mean  $\pm$  SD of triplicate measurements. Sub-G<sub>1</sub> phase indicates the cell population, in which DNA content was lower than that in the G<sub>0</sub>/G<sub>1</sub> phase. N/C, negative control; siRNA, small interfering RNA.

of the G<sub>2</sub>/M transition; therefore, the present study examined whether depletion of TFAP2E increased cell proliferation via suppressing TP53 expression. The data showed that knockdown of TFAP2E resulted in downregulation of TP53 at the protein level, but not at the mRNA level, in both Ca9-22 and HSC-4 cells (Fig. S4A and B). However, knockdown of TP53 using siRNA suppressed, rather than increased, the viability of both cells (Fig. S4C-F). These results indicate that accelerated proliferation of TFAP2E-knockdown cells could not owe to downregulation of the TP53 protein.

## Discussion

It has been reported that TFAP2E acts as a tumor suppressor in numerous types of cancer. For example, hypermethylation

of the TFAP2E genomic locus and reduced TFAP2E transcription have been shown to be associated with poor prognosis and resistance to treatment with 5-FU in patients with CRC and GC (15,16). Previously, we demonstrated that TFAP2E depletion in NB-derived cells attenuates the induction of cell death in response to adriamycin, CDDP or ionizing radiation (18). These findings indicated that TFAP2E exerts its tumor-suppressive effect by augmenting the response to DNA damage response in cancer cells. In the present study, silencing TFAP2E in OSCC-derived Ca9-22 and HSC-4 cells increased their proliferation but did not affect their sensitivity to CDDP or H<sub>2</sub>O<sub>2</sub>, indicating that TFAP2E knockdown did not affect DNA damage response in these cells.

The present study demonstrated that knockdown of TFAP2E increased the proliferation rate, rather than

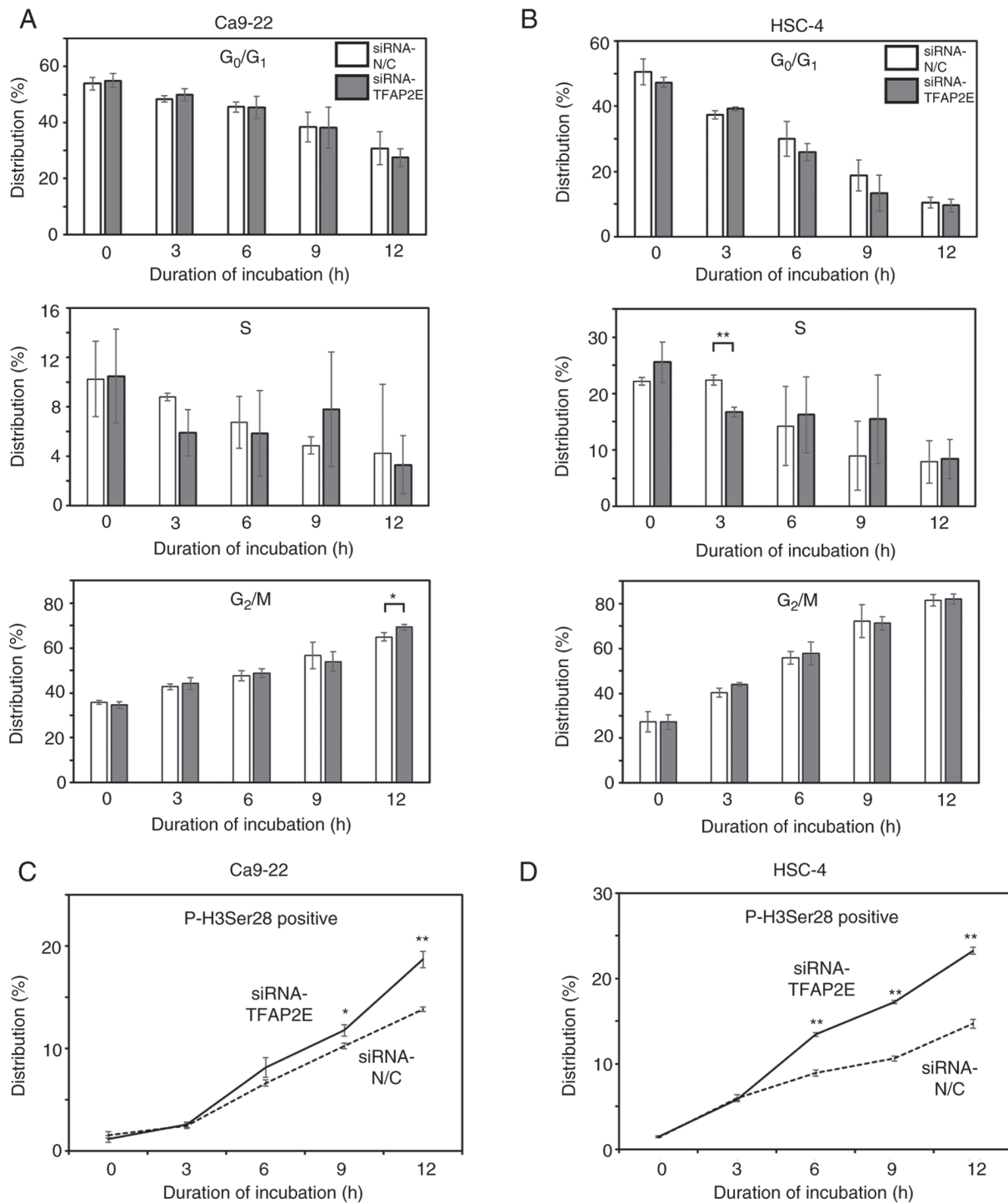


Figure 4. Knockdown of TFAP2E causes an earlier entry into M phase. (A and C) Ca9-22 and (B and D) HSC-4 cells were transfected with siRNA-TFAP2E or siRNA-N/C. A total of 2 days after transfection, the culture medium was replaced with fresh medium containing nocodazole. Both floating and adherent cells were harvested at the indicated time points and subjected to fluorescence-activated cell sorting analysis. (A and B) Percentage distribution was calculated based on Michael H. Fox algorithm. Data are presented as the means  $\pm$  SD of triplicate measurements. (C and D) Percentage of p-H3Ser28-positive cells. Data are presented as the mean  $\pm$  SD of triplicate measurements. \* $P < 0.05$ , \*\* $P < 0.01$  as indicated or vs. siRNA-N/C. N/C, negative control; siRNA, small interfering RNA.

suppressing cell death, in OSCC cells. There were no marked differences in cell cycle distribution pattern at certain time points or in the cell cycle progression rate from the G<sub>0</sub>/G<sub>1</sub> to G<sub>2</sub>/M in the presence of nocodazole between TFAP2E-knockdown cells and control cells. However, in the presence of nocodazole, the rate of increase in p-H3Ser28-positive cells was significantly higher in TFAP2E-depleted cells than that in the control group. Since

p-H3Ser28 is detectable at prophase/early anaphase during cell cycle progression (26), these observations suggested that TFAP2E may participate in the regulation of the G<sub>2</sub>/M transition, thereby contributing to the attenuation of OSCC cell proliferation. Cell cycle processes are guarded by cell cycle checkpoints, which survey DNA damage, DNA replication errors and incomplete spindle assembly (27,28). Errors in these processes induce cell cycle arrest or delay, thereby

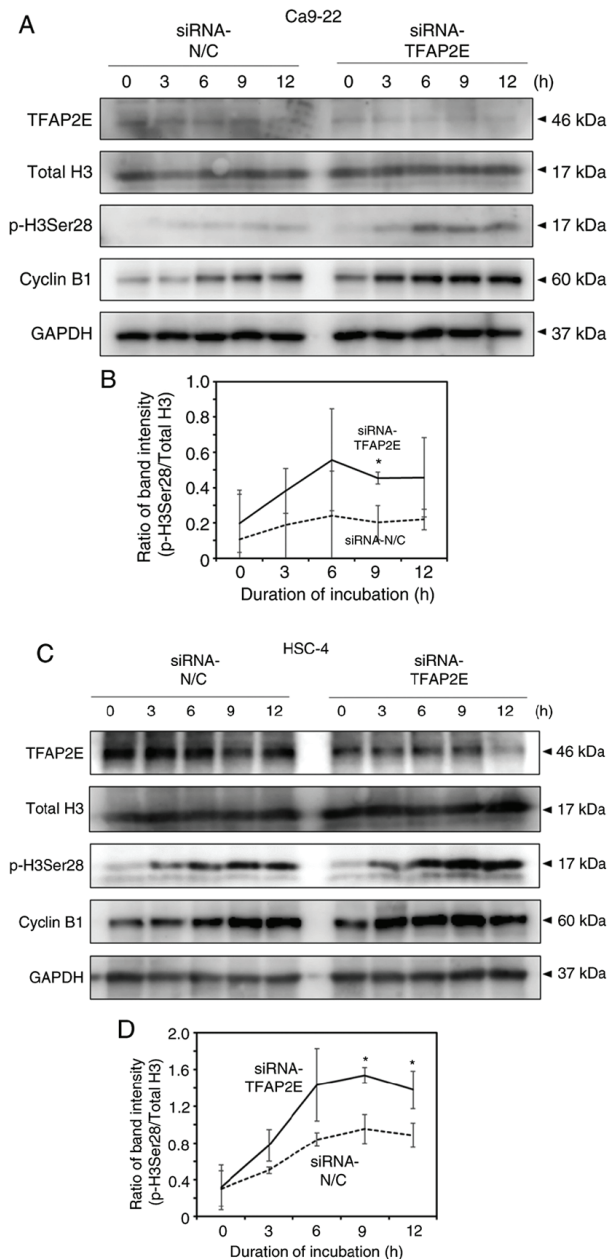


Figure 5. Accumulation of p-H3Ser28 and cyclin B1 is promoted in oral squamous cell carcinoma cells after TFAP2E knockdown compared with in the control group. (A) Ca9-22 and (C) HSC-4 cells were transfected with siRNA-TFAP2E or siRNA-N/C, and were treated with nocodazole 2 days after the transfection. Both floating and adherent cells were harvested at the indicated time points, and whole-cell lysates were subjected to western blotting analysis. GAPDH was used as a loading control. The band density of p-H3Ser28 was normalized to that of total H3 in (B) Ca9-22 and (D) HSC-4 cells. Data are presented as the mean  $\pm$  SD of triplicate measurements. \* $P < 0.05$  vs. siRNA-N/C. N/C, negative control; p-H3Ser28, phosphorylated histone H3 serine 28; siRNA, small interfering RNA.

preventing the accumulation and propagation of genetic errors during cell division. In the  $G_2$  phase, the checkpoint machinery can be activated by DNA damage, resulting in the inhibition of cyclin-dependent kinase 1 activity and preventing entry into mitosis (29). To clarify the molecular mechanisms by which TFAP2E may act during cell cycle progression, the expression levels and phosphorylation status of various functional proteins implicated in this process,

including PLK1, ATM, WEE1 and CDC25, were examined. The results showed that depletion of TFAP2E did not exhibit a marked effect on the expression or activation levels of these molecules (data not shown).

It is well established that the tumor suppressor molecule TP53 serves a pivotal role in regulating the  $G_2/M$  transition. TP53 induces cell cycle arrest at the  $G_1/S$  or  $G_2/M$  phase in response to various stresses through transactivation of a number of downstream target genes, including P21/WAF1, GADD45 and 14-3-3s (30). The present results showed that knockdown of TFAP2E in OSCC cells caused downregulation of TP53 at the protein level, but not the mRNA level, suggesting that TFAP2E may contribute to the stability of TP53. Ca9-22 and HSC-4 cells carry p53 mutations, R248W and R248Q, respectively, which have been reported to exhibit oncogenic functions (31,32). Predictably, depletion of TP53 suppressed, rather than increased, the proliferation rate of both cell lines, indicating that downregulation of the TP53 protein could not be responsible for the increased proliferation rate of TFAP2E-knockdown cells. Nevertheless, as the stability of mutant TP53 is regulated by multiple pathways (33), the observations presented in Fig. S4B suggest the involvement of TFAP2E in one of these pathways. Further investigations are required to identify the target molecules of TFAP2E and to elucidate the mechanisms underlying its regulatory effect on the cell cycle.

An important limitation of the present study is that all analyses were done using asynchronous cells. Although the results suggested that TFAP2E suppressed cell proliferation by regulating  $G_2/M$  transition, the possibility that there are other mechanisms by which TFAP2E affects cell proliferation cannot be ruled out. To verify this possibility, the analysis may need to be performed using phase-synchronized cells. Since we previously observed that anti-TFAP2E siRNA did not work in Ca9-22 and HSC-4 cells when they were treated with a double thymidine block protocol to synchronize the cell cycle (data not shown), we are planning to establish TFAP2E stable knockdown cells using short hairpin RNA. In addition, in our future work, other OSCC cell lines, such as HSC3 and UM-SCC6, in which anti-TFAP2E siRNA did not work (data not shown), will be tested. Another limitation of the present study is that the experiments were performed using only TFAP2E knockdown cells. Analysis of the effects of TFAP2E overexpression on OSCC cell function will provide further insight to understand its role in cell cycle regulation. In the future, we will establish TFAP2E-overexpressing OSCC cells along with knockdown cells, and will conduct a comprehensive analysis using those cells.

In conclusion, the present study showed that TFAP2E can suppress the proliferation of OSCC cells at least in part through regulating the  $G_2/M$  transition. This observation may explain the reason why patients with OSCC with lower TFAP2E expression had a shorter survival time.

#### Acknowledgments

The authors would like to thank Mr. Yushi Arai, Ms. Mayuko Yano and Mr. Shotaro Yoshida (Nihon University School of Dentistry) for technical assistance.



## Funding

This study was supported in part by KAKENHI (grant no. 22K17028) to YI, and by grants from the Dental Research Center, Nihon University School of Dentistry to Kyoko Fujiwara, and the Sato Fund, Nihon University School of Dentistry to KF.

## Availability of data and materials

The data generated in the present study may be requested from the corresponding author.

## Authors' contributions

RS and KF planned the experiments. RS, KF, ENM, YI, BY, EMF and YK performed the experiments. RS, KF, TT and SS wrote the manuscript. KF, ENM, SU, TK, TT and SS confirm the authenticity of all the raw data. KF, YI, SU, TK, TT and SS contributed to interpretation of the data. KF, SU, TK, TT and SS critically revised and approved for the paper for publication. All authors read and approved the final manuscript.

## Ethics approval and consent to participate

Not applicable.

## Patient consent for publication

Not applicable.

## Competing interests

The authors declare that they have no competing interests.

## References

- Sung H, Ferlay J, Siegel RL, Laversanne M, Soerjomataram I, Jemal A and Bray F: Global Cancer Statistics 2020: GLOBOCAN estimates of incidence and mortality worldwide for 36 cancers in 185 countries. *CA Cancer J Clin* 71: 209-249, 2021.
- Ferlay J, Soerjomataram I, Dikshit R, Eser S, Mathers C, Rebelo M, Parkin DM, Forman D and Bray F: Cancer incidence and mortality worldwide: Sources, methods and major patterns in GLOBOCAN 2012. *Int J Cancer* 136: E359-E386, 2015.
- National Cancer Institute: SEER Cancer Statistics Review (CSR) 1975-2018. NCI, Bethesda, MD, 2021. [https://seer.cancer.gov/csr/1975\\_2018/](https://seer.cancer.gov/csr/1975_2018/).
- Kumar M, Nanavati R, Modi TG and Dobariya C: Oral cancer: Etiology and risk factors: A review. *J Cancer Res Ther* 12: 458-463, 2016.
- Cancer Genome Atlas Network: Comprehensive genomic characterization of head and neck squamous cell carcinomas. *Nature* 517: 576-582, 2015.
- Fujiwara K, Ghosh S, Liang P, Morien E, Soma M and Nagase H: Genome-wide screening of aberrant DNA methylation which associated with gene expression in mouse skin cancers. *Mol Carcinog* 54: 178-188, 2015.
- Kolat D, Kaluzi Nska Z, Bednarek AK and Zbieta Pluciennik E: The biological characteristics of transcription factors AP-2 $\alpha$  and AP-2 $\gamma$  and their importance in various types of cancers. *Biosci Rep* 39: BSR20181928, 2019.
- Eckert D, Buhl S, Weber S, Jäger R and Schorle H: The AP-2 family of transcription factors. *Genome Biol* 6: 246, 2005.
- Wang HV, Vaupel K, Buettner R, Bosserhoff AK and Moser M: Identification and embryonic expression of a new AP-2 transcription factor, AP-2 epsilon. *Dev Dyn* 231: 128-135, 2004.
- Feng W, Simoes-de-Souza F, Finger TE, Restrepo D and Williams T: Disorganized olfactory bulb lamination in mice deficient for transcription factor AP-2epsilon. *Mol Cell Neurosci* 42: 161-171, 2009.
- Jain S, Glubrecht DD, Germain DR, Moser M and Godbout R: AP-2 $\epsilon$  Expression in developing retina: Contributing to the molecular diversity of amacrine cells. *Sci Rep* 8: 3386, 2018.
- Wenke AK, Grä Ssel S, Moser M and Bosserhoff AK: The cartilage-specific transcription factor Sox9 regulates AP-2 $\epsilon$  expression in chondrocytes. *FEBS J* 276: 2494-2504, 2009.
- Wenke AK, Rothhammer T, Moser M and Bosserhoff AK: Regulation of integrin  $\alpha$ 10 expression in chondrocytes by the transcription factors AP-2epsilon and Ets-1. *Biochem Biophys Res Commun* 345: 495-501, 2006.
- Giaretti W, Molinu S, Ceccarelli J and Prevosto C: Chromosomal instability, aneuploidy, and gene mutations in human sporadic colorectal adenomas. *Cell Oncol* 26: 301-305, 2004.
- Ebert MP, Tänzer M, Balluff B, Burgermeister E, Kretzschmar AK, Hughes DJ, Tetzner R, Lofton-Day C, Rosenberg R, Reinacher-Schick AC, *et al*: TFAP2E-DKK4 and chemoresistance in colorectal cancer. *N Engl J Med* 366: 44-53, 2012.
- Sun J, Du N, Li J, Zhou J, Tao G, Sun S and He J: Transcription Factor AP2 $\epsilon$ : A potential predictor of chemoresistance in patients with gastric cancer. *Technol Cancer Res Treat* 15: 285-295, 2016.
- Payne SR, Serth J, Schostak M, Kamradt J, Strauss A, Thelen P, Model F, Day JK, Liebenberg V, Morotti A, *et al*: DNA methylation biomarkers of prostate cancer: Confirmation of candidates and evidence urine is the most sensitive body fluid for non-invasive detection. *Prostate* 69: 1257-1269, 2009.
- Hoshi R, Watanabe Y, Ishizuka Y, Hirano T, Nagasaki-Maeoka E, Yoshizawa S, Uekusa S, Kawashima H, Ohashi K, Sugito K, *et al*: Depletion of TFAP2E attenuates adriamycin-mediated apoptosis in human neuroblastoma cells. *Oncol Rep* 37: 2459-2464, 2017.
- Zhao M, Sano D, Pickering CR, Jasser SA, Henderson YC, Clayman GL, Sturgis EM, Ow TJ, Lotan R, Carey TE, *et al*: Assembly and initial characterization of a panel of 85 genomically validated cell lines from diverse head and neck tumor sites. *Clin Cancer Res* 17: 7248-7264, 2011.
- Jordan MA, Thrower D and Wilson L: Effects of vinblastine, podophyllotoxin and nocodazole on mitotic spindles. Implications for the role of microtubule dynamics in mitosis. *J Cell Sci* 102 (Pt 3): 401-416, 1992.
- Fox MH: A model for the computer analysis of synchronous DNA distributions obtained by flow cytometry. *Cytometry* 1: 71-77, 1980.
- Larionov A, Krause A and Miller W: A standard curve based method for relative real time PCR data processing. *BMC Bioinformatics* 6: 62, 2005.
- Thellin O, Zorzi W, Lakaye B, De Borman B, Coumans B, Hennen G, Grisar T, Igout A and Heinen E: Housekeeping genes as internal standards: Use and limits. *J Biotechnol* 75: 291-295, 1999.
- Schneider CA, Rasband WS and Eliceiri KW: NIH Image to ImageJ: 25 years of image analysis. *Nat Methods* 9: 971-675, 2012.
- Sherman J and Wang R: Rapid profiling of G2 phase to mitosis progression by flow cytometry in asynchronous cells. *Cell Cycle* 19: 2897-2905, 2020.
- Pérez-Cadahía B, Drobic B and Davie JR: H3 phosphorylation: Dual role in mitosis and interphase. *Biochem Cell Biol* 87: 695-709, 2009.
- De Wever V, Lloyd VC, Nasa I, Nimick I and Trinkle-Mulcahy M, Gourlay R, Morrice N and Moorhead GB: Isolation of human mitotic protein phosphatase complexes: Identification of a complex between protein phosphatase 1 and the RNA helicase Ddx21. *PLoS One* 7: e39510, 2012.
- Matthews HK, Bertoli C and de Bruin RAM: Cell cycle control in cancer. *Nat Rev Mol Cell Biol* 23: 74-88, 2022.
- Medema RH and Macurek L: Checkpoint control and cancer. *Oncogene* 31: 2601-2613, 2012.
- Stark GR and Taylor WR: Control of the G2/M transition. *Mol Biotechnol* 32: 227-248, 2006.
- Yan W and Chen X: Characterization of functional domains necessary for mutant p53 gain of function. *J Biol Chem* 285: 14229-14238, 2010.
- Ng JW, Lama D, Lukman S, Lane DP, Verma CS and Sim AY: R248Q mutation-Beyond p53-DNA binding. *Proteins* 83: 2240-2250, 2015.
- Wang J, Liu W, Zhang L and Zhang J: Targeting mutant p53 stabilization for cancer therapy. *Front Pharmacol* 14: 1215995, 2023.

